

Scale-dependent statistics of inertial particle distribution in high Reynolds number turbulence

Keigo Matsuda ^{1,*}, Kai Schneider ², and Katsunori Yoshimatsu ³

¹Research Institute for Value-Added-Information Generation (VAiG), Japan Agency for Marine-Earth Science and Technology (JAMSTEC), Yokohama 236-0001, Japan

²Institut de Mathématiques de Marseille (I2M), Aix-Marseille Université, CNRS and Centrale Marseille, 39 Rue F. Joliot-Curie, 13453 Marseille Cedex 13, France

³Institute of Materials and Systems for Sustainability, Nagoya University, Nagoya 464-8601, Japan



(Received 20 July 2020; accepted 17 May 2021; published 9 June 2021)

Multiscale statistical analyses of inertial particle distributions are presented to investigate the statistical signature of clustering and void regions in particle-laden incompressible isotropic turbulence. Three-dimensional direct numerical simulations of homogeneous isotropic turbulence at high Reynolds number ($Re_\lambda \gtrsim 200$) are performed. Lagrangian motion of inertial particles are tracked by the one-way coupled point-particle method assuming the Stokes drag. Up to 10^9 inertial particles for each Stokes number ranging from 0.01 to 5.0 are computed. Orthogonal wavelet analysis is then applied to the computed particle-number density fields. Scale-dependent skewness and flatness values of the particle-number density distributions are calculated and the influence of Reynolds number Re_λ and Stokes number St is assessed. For $St \sim 1$, both the scale-dependent skewness and flatness values become larger as the scale decreases, suggesting intermittent clustering at small scales. For $St \leq 0.2$, the flatness at intermediate scales, i.e., scales larger than the Kolmogorov scale and smaller than the integral scale of the flow, increases as St increases, and the skewness exhibits negative values at the intermediate scales. The negative values of the skewness are a signature of void regions. These results indicate that void regions at the intermediate scales are pronounced and intermittently distributed for such small Stokes numbers. As Re_λ increases, the flatness increases weakly. For $Re_\lambda \geq 328$, the skewness shows negative values at large scales, suggesting that even for $St \sim 1$, void regions are pronounced at large scales, while clusters are pronounced at small scales.

DOI: [10.1103/PhysRevFluids.6.064304](https://doi.org/10.1103/PhysRevFluids.6.064304)

I. INTRODUCTION

Inertial particles suspended in three-dimensional (3D) turbulent flows are ubiquitous in geophysical flows. The spectrum of applications covers plankton dynamics, pollution dispersion in cities or in the atmosphere, or even the planet formation in the early age of our universe. The precipitation mechanism in convective clouds, where inertial particles (i.e., water droplets) are suspended in high Reynolds number turbulence, is of particular interest in atmospheric flow [1]. For instance, cloud droplet motion in turbulence increases the collision coalescence frequency and enhances the rain drop formation. The importance of turbulence in the collision coalescence process is well summarized in the introduction of Ref. [2]. One of the key factors that determines the droplet collision coalescence frequency is turbulent clustering of cloud droplets. Due to the inertia of cloud droplets, their motion deviates from turbulent flow motion and particles form

*k.matsuda@jamstec.go.jp

a nonuniform number density distribution. The distribution consists of cluster and void regions, which, respectively, correspond to large and small number densities. Clustering of cloud droplets can also increase the radar reflectivity factor [3,4] due to the interference of microwaves scattered by spatially correlated droplets. Quantitative estimates of the increase in the radar reflectivity factor require the Fourier spectrum of number density fluctuations of turbulent clustering particles which covers scales comparable to radar wavelengths. Sound modeling becomes necessary for improving weather prediction. However, investigation of particle dynamics in high Reynolds number turbulence, like cloud turbulence, is still challenging for *in situ* observations, laboratory experiments, and numerical simulations. Understanding the nonlinear multiscale dynamics is a prerequisite for estimating and modeling intermittent particle clustering in high Reynolds number turbulence.

Inertial particle clustering in homogeneous isotropic turbulence was investigated in many publications. For review articles on this topic, we refer readers to, e.g., Refs. [5,6]. In this paper, we consider inertial heavy particles; i.e., the particle density is sufficiently larger than the fluid density. When the particle size is smaller than the smallest turbulent length scale, i.e., the Kolmogorov scale, the particle acceleration balances the drag force, which is inversely proportional to the particle relaxation time, τ_p [2,7,8]. A dimensionless parameter for τ_p is the Stokes number, which is defined as $St \equiv \tau_p/\tau_\eta$, where τ_η is the Kolmogorov time. The clustering of inertial heavy particles was first explained by the preferential concentration mechanism [9,10], in which inertial particles are swept out from strong vortices due to centrifugal effects and concentrate in low-vorticity and high-strain-rate regions when the particle relaxation time is sufficiently small compared to the time scale of vortices.

Many previous studies were motivated to quantify the collision coalescence process (e.g., Refs. [2,11–21]) and discussed clustering mainly at sub-Kolmogorov scales. The radial distribution function (RDF) is widely used to analyze clustering (e.g., Refs. [2,16,20,22]) because it is directly related with the particle collision rate [11,23]. The RDF typically shows a power-law behavior at sub-Kolmogorov scales and the slope (i.e., the correlation dimension [24]) is dependent on the Stokes number St . Ireland *et al.* [2] discussed the Reynolds number dependence of the RDF at sub-Kolmogorov scales by performing 3D direct numerical simulations (DNSs) for a wide range of Reynolds numbers, $88 \leq Re_\lambda \leq 597$, where Re_λ is the Taylor-microscale-based Reynolds number. They stated that the RDF is independent of Re_λ for small Stokes numbers, and the clustering mechanism is driven almost entirely by small-scale turbulence. In contrast to the conclusion in Ref. [2], Onishi *et al.* [25] showed that the RDF for $St = 0.4$ decreases when increasing the Reynolds number for $Re_\lambda > 100$ by performing 3D DNSs for $55 \leq Re_\lambda \leq 527$. By comparing with 2D turbulence, Onishi and Vassilicos [20] revealed that the Reynolds number dependence of the RDF in 3D turbulence is due to the intermittent nature of turbulence, which corresponds to non-Gaussianity of turbulent fluctuations.

To discuss the intermittent particle clustering in high Reynolds number turbulence, understanding multiscale particle clustering structures at scales larger than the Kolmogorov scale is crucial. Multiscale structures of inertial particle clustering have been reported in many previous studies. Boffetta *et al.* [26] pointed out that a multiscale structure of clustering can be observed in the inverse cascade range in two-dimensional turbulence. They showed that the probability density function (PDF) of void area exhibits a power-law, independent of the Stokes number. Yoshimoto and Goto [27] reported similar results for the PDF of void volumes at scales larger than the Kolmogorov scale in homogeneous isotropic turbulence using 3D DNS. The multiscale structure of clustering was also observed in experiments by Monchaux *et al.* [28]: They measured particle distribution in a wind tunnel and reported that both PDFs of void and cluster areas exhibit power laws independent of the Stokes number. The multiscale clustering structure was also analyzed using the pair correlation function (PCF) [27,29] and its Fourier transform, which is the Fourier spectrum of number density fluctuations [3]. It was shown that both the PCF and the Fourier spectrum are strongly dependent on the Stokes numbers even at scales larger than the Kolmogorov scale. The multiscale structures of inertial particle clustering are explained by the advection in turbulent flows

and the deviation from the fluid flows due to the inertial effects. The advection of particles results in the turbulent transport of particle number density fields at sufficiently large scales. However, the turbulent transport of passive scalar [30] is not directly applicable to discuss the multiscale structure of inertial particle clustering [31]. Vassilicos and coworkers explained the scale similarity of particle distribution, proposing the sweep-stick mechanism, in which particles are swept by large-scale flow motion while sticking to stagnation points of Lagrangian fluid acceleration [32–35]. Bec *et al.* [24] discussed the scale dependence of particle distribution, using the PDF of particle mass density, coarse grained on scales in the inertial range based on their 3D DNS data. They reported that the PDF changes with the scale-dependent contraction rate. Attempts to formulate the scale similarity of particle clustering in the inertial range of turbulence have been done by Bragg *et al.* [36] and Ariki *et al.* [31] on the basis of theoretical analyses. They proposed analytical estimates assuming Gaussianity of particle-number density fluctuations. Assessing the non-Gaussianity of scale-by-scale spatial fluctuation is a prerequisite for further development of the analytical estimates.

Wavelet analysis is a suitable tool to quantify the multiscale non-Gaussianity based on the scale-dependent spatial statistics of particle number density fields. We consider continuous number density fields constructed from Lagrangian particle distributions. Wavelets represent turbulent fields (such as flow, scalar, and particle-number density fields) localized in scale and position (and possibly direction), complementary to Fourier techniques which yield insight into wave-number contributions of turbulent fields. Hence the wavelet representation can quantify spatial fluctuations at different scales, which is a key for analyzing scale-dependent spatial statistics of number density fields. This is possible due to the local and oscillatory character of the wavelet basis functions which yield an efficient orthogonal representation of the field. The efficient processing is realized thanks to the fast wavelet transform which has linear computational complexity. For the Fourier transform, this task is out of reach owing to the global character of the basis functions. Wavelet techniques for turbulent flow already have some history, starting with the work of, e.g., Refs. [37–39]. Numerous applications can be found to extract coherent vorticity [40–42], quantifying intermittency [43,44], performing scale-dependent statistics [45] and turbulence modeling [46,47]. A review for computing turbulent flows can be found in Ref. [48]. Recently, orthogonal wavelets have been applied to active matter turbulence [49], turbulent premixed combustion [50], and droplet-laden turbulence [51]. Wavelets have also been applied to the number density fields for inertial particles in turbulence. Bassenne *et al.* [52] proposed a wavelet-based method to extract coherent clusters of inertial particles in fully developed turbulence, and a grid adaptation method using wavelet analysis was illustrated. They studied Fourier energy spectra for several Stokes numbers, analyzing the impact when changing the number of particles. Wavelet multiresolution statistics of particle-laden turbulence have been recently introduced in Ref. [53] for studying the cross correlations between energy spectra of the fluid and the dispersed-phase field variables in particle-laden turbulence. These studies of wavelet statistics for particle clustering mainly focused on the second-order scale-dependent statistics and its spatial variance.

The aim of the current paper is to study the scale-dependent statistics of the intermittent particle distribution and get insight into the multiscale structure of clusters and voids in particle-laden turbulence. Higher-order scale-dependent statistics (i.e., higher than second order) are necessary to understand the intermittent nature of particle distribution and how void and cluster regions contribute to the particle clustering. To this end, orthogonal wavelet decomposition of the particle number density fields is performed. The analyzed data are obtained by DNSs of 3D homogeneous isotropic turbulence at high Reynolds number laden with inertial particles, where $Re_\lambda \gtrsim 200$. The influence of different physical parameters, Reynolds number Re_λ , and Stokes number St , is assessed.

The remainder of the paper is organized as follows. First, we briefly summarize the governing equations and the performed DNS computations in Sec. II. In Sec. III, we describe the wavelet methodology and wavelet-based statistical measures to quantify the scale-dependent distribution of the particle number density field. Numerical results are then presented in Sec. IV. Finally, Sec. V draws some conclusions and gives perspectives for future work.

II. PARTICLE-LADEN TURBULENCE

We present the governing equations of particle-laden turbulence in Sec. II A, and describe the DNS computations in Sec. II B. In Sec. II C, we explain the conversion of the Lagrangian particle data into an Eulerian number density field.

A. Basic equations

We consider a statistically homogeneous velocity field $\mathbf{u}(\mathbf{x}, t)$ of an incompressible fluid obeying the Navier–Stokes equation together with the divergence-free condition,

$$\frac{\partial \mathbf{u}}{\partial t} + (\mathbf{u} \cdot \nabla) \mathbf{u} = -\frac{1}{\rho} \nabla p + \nu \nabla^2 \mathbf{u} + \mathbf{f}, \quad (1)$$

$$\nabla \cdot \mathbf{u} = 0, \quad (2)$$

where $\mathbf{x} = (x_1, x_2, x_3)$, $\nabla = (\partial/\partial x_1, \partial/\partial x_2, \partial/\partial x_3)$, t is the time, $\mathbf{f}(\mathbf{x}, t)$ is an external solenoidal forcing, $p(\mathbf{x}, t)$ is the pressure, ν is the kinematic viscosity of the fluid, and ρ is the density. The equations are completed with periodic boundary conditions and a suitable initial condition. Here and in the following, we omit the arguments \mathbf{x} and t , unless otherwise stated.

We assume that the particle size is sufficiently smaller than the Kolmogorov scale and the particle density ρ_p is sufficiently larger than the fluid density ρ (i.e., $\rho_p/\rho \gg 1$). Then, on the basis of the point-particle approximation, Lagrangian motion of inertial heavy particles [2,7,8] can be described by

$$\frac{d\mathbf{x}_p}{dt} = \mathbf{v}, \quad (3)$$

$$\frac{d\mathbf{v}}{dt} = -\frac{\mathbf{v} - \mathbf{u}}{\tau_p}, \quad (4)$$

where \mathbf{x}_p and \mathbf{v} are the position and velocity of a Lagrangian particle and τ_p is the relaxation time of particle motion. Assuming the Stokes flow for a spherical particle (i.e., the Stokes drag), τ_p is given by

$$\tau_p = \frac{\rho_p}{\rho} \frac{2a^2}{9\nu}, \quad (5)$$

where a is the particle radius. The Stokes drag is valid for $\text{Re}_p \leq 0.1$ but is often relaxed to $\text{Re}_p \leq 1$, where $\text{Re}_p = 2a|\mathbf{u} - \mathbf{v}|/\nu$ is the particle Reynolds number, cf. the discussion in Ref. [54].

The important parameters in this paper are the Taylor-microscale based Reynolds number Re_λ and the Stokes number St . The Taylor-microscale-based Reynolds number Re_λ is defined as $\text{Re}_\lambda \equiv u'\lambda/\nu$, where u' is the turbulent velocity fluctuation $u' \equiv \sqrt{\langle |\mathbf{u}|^2 \rangle / 3}$ and λ is the Taylor microscale $\lambda \equiv \sqrt{15\nu u'^2/\epsilon}$. ϵ is the energy dissipation rate, defined by $\epsilon \equiv \nu \langle \frac{\partial u_i}{\partial x_j} \frac{\partial u_i}{\partial x_j} \rangle$ and $\langle \cdot \rangle$ denotes an ensemble average. The Stokes number St indicates the contribution of particle inertia and defined as $\text{St} \equiv \tau_p/\tau_\eta$, where τ_η is the Kolmogorov time ($\tau_\eta \equiv \sqrt{\nu/\epsilon}$). In homogeneous turbulence, the ensemble average can be regarded as a space and time average under appropriate assumptions.

In the equations above, we assumed that the effects of the reaction of particle motion to fluid flow and the interactions between particles were neglected (i.e., one-way coupling) because these effects are typically small in the timescale of τ_η for sufficiently dilute particles such as cloud droplets in atmospheric turbulence [4].

B. Direct numerical simulation

The DNS of particle-laden turbulence was performed using the same DNS program as used in Ref. [3]. Equations (1) and (2) were solved on Cartesian staggered grids. The fourth-order central-difference schemes were used for the advection and viscous terms [55] and the second-order

TABLE I. DNS parameters and statistics of obtained turbulence, the number of grid points N_{grid} , the Reynolds number of DNS $\text{Re} = \nu^{-1}$, the Taylor-microscale based Reynolds number Re_λ , the turbulent velocity fluctuation u' , $k_{\text{max}}\eta$, the number of particles N_p , the particle relaxation time τ_p , the Stokes number $\text{St} \equiv \tau_p/\tau_\eta$, and the time step Δt .

	N_{grid}	Re	Re_λ	u'	$k_{\text{max}}\eta$	N_p	τ_p	St	Δt
Flow 1	512	909	204	1.01	2.02	1.07×10^9	5.71×10^{-4}	0.01	2×10^{-4}
							1.14×10^{-3}	0.02	
							2.86×10^{-3}	0.05	1×10^{-3}
							5.71×10^{-3}	0.1	
							1.14×10^{-2}	0.2	
							2.86×10^{-2}	0.5	
							5.71×10^{-2}	1.0	
							1.14×10^{-1}	2.0	
2.86×10^{-1}	5.0								
Flow 2	1024	2220	328	1.00	2.12	5.00×10^7	3.87×10^{-2}	1.0	2×10^{-4}
Flow 3	2048	5595	531	1.00	2.14	4.00×10^8	2.52×10^{-2}	1.0	1×10^{-4}

Runge–Kutta scheme was used for time integration. The velocity and pressure were coupled by the highly simplified marker and cell method [56], where the second-order central difference scheme was used for the pressure gradient. To obtain statistically steady-state turbulence, a parallelized external solenoidal forcing [57] was applied to the large scales satisfying $k < 2.5$. Here $k = |\mathbf{k}|$ is a magnitude of wave number vector \mathbf{k} . Equations (3) and (4) were solved for discrete Lagrangian points. The time integration scheme was the same as that for the flow field.

The computational cubic domain has side length of 2π . Periodic boundary conditions are applied in x_1 , x_2 , and x_3 directions. The domain was discretized uniformly into N_{grid}^3 grid points, giving a grid spacing of $\Delta = 2\pi/N_{\text{grid}}$. The DNS was performed for three turbulent flows at different Reynolds numbers: Flow 1, flow 2, and flow 3. The resolution was chosen to satisfy $k_{\text{max}}\eta \approx 2$, where k_{max} is the maximum wave number given by $k_{\text{max}} = \pi/\Delta$ and $\eta = (\nu^3/\epsilon)^{1/4}$ is the Kolmogorov scale. Inertial particles were imposed uniformly and randomly in the computational domain at $t = 0$, where the turbulent flow field had reached a statistically steady state. Particle position data were sampled at 10 time instants of $t = 11T_0$ to $20T_0$ at interval of T_0 , where T_0 is the dimensionless time unit and comparable to the eddy-turnover time. The Stokes number St of inertial particles was set to 0.01, 0.02, 0.05, 0.1, 0.2, 0.5, 1.0, 2.0 and 5.0 for flow 1, and the particle motion of $\text{St} = 1.0$ was tracked for flow 2 and flow 3. The statistics of the obtained turbulent flows and the number of particles N_p are summarized in Table I. Note that N_p particles were tracked for each case of St for flow 1. Time average for the statistics was taken for the period of $10T_0 \leq t \leq 20T_0$. The time step Δt for $\text{St} = 0.01$ and 0.02 in flow 1 is smaller than that for $0.05 \leq \text{St} \leq 5.0$ so that it is smaller than τ_p . We confirmed that the statistics of turbulence and particle clustering do not change when Δt is decreased to one-fifth (figures are omitted for brevity).

Since the one-way coupling is assumed in this paper, each particle motion is independent of the number of particles. The physics relevant to inertial particle clustering does not differ from the sufficiently dilute condition even when increasing the number of particles. Thus, we use a huge number of particles to reduce influence of the Poisson noise, particularly for flow 1. We note that the particle number density for flow 1 is much larger than that in real cloud turbulence. When we consider water droplets in air flow, where $\rho_p/\rho = 840$ at 1 atm and 298 K, the particle mass and volume fractions for $\text{St} = 1.0$ in flow 1 are 2.9 and 3.5×10^{-3} , respectively. This implies that if the particle number density were the same as that of flow 1, the effects of the reaction of particle motion onto the flow and the interaction between particles would not be negligibly small.

It should also be noted that, when we consider cloud droplets with $\rho_p/\rho = 840$, the root mean square of the particle Reynolds number Re_p for $\text{St} \leq 0.2$ becomes smaller than 0.03, and it becomes

0.11, 0.26, 0.62, and 1.7 for $St = 0.5, 1.0, 2.0,$ and $5.0,$ respectively. For $St = 5.0,$ the DNS results may not be directly applied to cloud droplets. We included $St = 5.0$ because Re_p depends on the particle size $a/\eta = \sqrt{9St/(2\rho_p/\rho)}$ and can be smaller than 1 when ρ_p/ρ is sufficiently large.

C. Number density fluctuations

The number density field of the discrete particle positions can be described as

$$n_\delta(\mathbf{x}, t) = \frac{1}{n_0} \sum_{m=1}^{N_p} \delta(\mathbf{x} - \mathbf{x}_{p,m}(t)), \quad (6)$$

where $\delta(\mathbf{x})$ is the Dirac delta function, the subscript m denotes the identification number of the particle, and n_0 is the scaling factor: The mean dimensional number density $n_0 = N_p/(2\pi)^3$ is used so that $\langle n_\delta \rangle = 1$. However, wavelet analysis cannot be applied directly to $n_\delta(\mathbf{x}, t)$. Thus, to apply the wavelet analysis, the number density field in Eq. (6) was converted to the number density field data on equidistant grid points based on the histogram method; i.e., the computational domain was discretized into an array of N_g^3 equally sized boxes and the number of particles in each box was counted. The histogram method, which corresponds to the zeroth-order kernel density estimation, retains fine clustering structures better than higher-order kernels. The number density field based on the histogram method is given by

$$n(\mathbf{x}, t) = \sum_{i_1, i_2, i_3=0}^{N_g-1} \left\{ \int_{\mathbb{T}^3} K_h(\mathbf{x}_{i_1, i_2, i_3} - \mathbf{x}') n_\delta(\mathbf{x}', t) d\mathbf{x}' \right\} h^3 K_h(\mathbf{x} - \mathbf{x}_{i_1, i_2, i_3}), \quad (7)$$

where $\mathbb{T} = 2\pi\mathbb{R}/\mathbb{Z}$, $\mathbf{x}_{i_1, i_2, i_3}$ is the box position given by $\mathbf{x}_{i_1, i_2, i_3} = h(i_1 + 1/2, i_2 + 1/2, i_3 + 1/2)$ and $K_h(\mathbf{x})$ is a piecewise constant function defined as $K_h(\mathbf{x}) = 1/h^3$ for $-h/2 \leq x_i < h/2$ ($i = 1, 2, 3$), while $K_h(\mathbf{x}) = 0$ otherwise. Here h denotes the width of the piecewise function, and for the histogram we have $h = 2\pi/N_g$. Note that Eq. (7) satisfies $\langle n \rangle = 1$. For the number density field $n(\mathbf{x}, t)$, the number of grid points in each direction was set to $N_g = 1024$, independently of the number of grid points N_{grid} in the DNS. The influence of N_g on the wavelet-based statistics is discussed in Appendix B. Bassenne *et al.* [52] also used the histogram method to obtain the number density field for the wavelet analysis. Nguyen *et al.* [58] used the kernel density estimation with the Gaussian kernel but the Gaussian kernel smooths out fine clustering structures because it works as a blunt low-pass filter.

III. WAVELET ANALYSIS OF THE NUMBER DENSITY FIELD

The scale-dependent statistics of the particle number density field $n(\mathbf{x}, t)$, Eq. (7), are based on an orthogonal wavelet decomposition which is summarized in Sec. III A. For details on wavelets, we refer the reader to textbooks, e.g., Refs. [59,60]. The scale-dependent moments of the number density field yield statistical estimators of the different quantities considered, such as variance, skewness, and flatness values, and are defined in Sec. III B.

A. Orthogonal wavelet decomposition

We consider here a scalar field $n(\mathbf{x}, t)$, i.e., the particle number density field at a given instant t , in the $(2\pi)^3$ periodic cube. The field is decomposed into a 3D orthogonal wavelet series, and it is thus unfolded into scale, position, and seven directions ($\mu = 1, \dots, 7$). The 3D mother wavelet $\psi_\mu(\mathbf{x})$ is hereby based on a tensor product construction and a family of wavelets $\psi_{\mu, \boldsymbol{\gamma}}(\mathbf{x})$ can be generated by dilation and translation. This family yields an orthogonal basis of $L^2(\mathbb{R}^3)$. The multi-index $\boldsymbol{\gamma} = (j, i_1, i_2, i_3)$ denotes the scale 2^{-j} and position $2\pi \times 2^{-j} \mathbf{i} = 2\pi \times 2^{-j} (i_1, i_2, i_3)$ of the wavelets for each direction, and $i_\ell = 0, \dots, 2^j - 1$ ($\ell = 1, 2, 3$). The wavelets are well-localized in space around position $2\pi \times 2^{-j} \mathbf{i}$ and scale 2^{-j} , oscillating, and smooth. Application of a periodization

technique [60] to the wavelets likewise generates an orthogonal basis of $L^2(\mathbb{T}^3)$. The spatial average of $\psi_{\mu,\gamma}(\mathbf{x})$, defined by $\langle \psi_{\mu,\gamma} \rangle = (2\pi)^{-3} \int_{\mathbb{T}^3} \psi_{\mu,\gamma}(\mathbf{x}) d\mathbf{x}$, vanishes for each index, which is a necessary condition for being a wavelet.

The number density field $n(\mathbf{x})$ sampled on $N_g^3 = 2^{3j}$ equidistant grid points can be developed into an orthogonal wavelet series,

$$n(\mathbf{x}) = \langle n(\mathbf{x}) \rangle + \sum_{j=0}^{J-1} n_j(\mathbf{x}), \quad (8)$$

where $n_j(\mathbf{x})$ is the contribution of $n(\mathbf{x})$ at scale 2^{-j} defined by

$$n_j(\mathbf{x}) = \sum_{\mu=1}^7 \sum_{i_1, i_2, i_3=0}^{2^j-1} \tilde{n}_{\mu,\gamma} \psi_{\mu,\gamma}(\mathbf{x}), \quad (9)$$

and $\langle n(\mathbf{x}) \rangle$ is the mean value. Due to orthogonality of the wavelets, the coefficients are given by $\tilde{n}_{\mu,\gamma} = \langle n, \psi_{\mu,\gamma} \rangle$, where $\langle \cdot, \cdot \rangle$ denotes the L^2 -inner product defined by $\langle \xi, \zeta \rangle = (2\pi)^{-3} \int_{\mathbb{T}^3} \xi(\mathbf{x}) \zeta(\mathbf{x}) d\mathbf{x}$. At scale 2^{-j} , we have 7×2^{3j} wavelet coefficients for $n(\mathbf{x})$. Thus, in total we have $N_g^3 - 1$ wavelet coefficients and the nonvanishing mean value. These coefficients are efficiently computed from the N_g^3 grid point values for $n(\mathbf{x})$ using the fast wavelet transform, which has linear computational complexity.

The scale 2^{-j} of the wavelet transform and the wave number k_j of the Fourier transform are related via

$$k_j = k_\psi 2^j, \quad (10)$$

where k_ψ is the centroid wave number of the chosen wavelet. For the Coiflet 12 wavelet chosen here, which has four vanishing moments, we have $k_\psi = 0.77$.

B. Wavelet-based statistics of the particle number density field

Scale-dependent statistics of the particle number density field $n(\mathbf{x})$ are defined by using scale-dependent moments based on the wavelet decomposition of Eq. (8). We define the q th-order moments of $n_j(\mathbf{x})$ as

$$M_q[n_j] = \langle (n_j)^q \rangle, \quad (11)$$

and note that by construction the mean value vanishes, $\langle n_j \rangle = 0$. The moments are thus central moments. These scale-dependent moments are intimately related to the q th-order structure functions [43].

In the following, we consider the second-order moment $M_2[n_j]$, the third-order moment $M_3[n_j]$, and the fourth-order moment $M_4[n_j]$. The wavelet energy spectrum of $n_j(\mathbf{x})$ can be defined using the second-order moment $M_2[n_j]$ and Eq. (10),

$$E[n_j] = \frac{1}{\Delta k_j} M_2[n_j], \quad (12)$$

where $\Delta k_j = (k_{j+1} - k_j) \ln 2$ [39]. The wavelet spectrum $E[n_j]$ corresponds to a smoothed version of the Fourier energy spectrum [38,39]. The orthogonality of the wavelets implies that we obtain the variance of the number density field from $\sum_{j=0}^{J-1} E[n_j] \Delta k_j$. Similarly to the Fourier spectra reported by Bassenne *et al.* [52], the energy spectrum obtained by Eq. (12) has the particle-number dependence due to the Poisson noise. In this paper, we have analytically obtained the effect of the Poisson noise on $M_2[n_j]$, which is given by

$$M_{2,\text{random}}[n_j] = \frac{7 \cdot 2^{3j}}{N_p}. \quad (13)$$

The details on the analytical procedure are summarized in Appendix A. Hence, instead of Eq. (12), we use the following definition for the wavelet energy spectrum:

$$E[n_j] = \frac{1}{\Delta k_j} \left\{ M_2[n_j] - \frac{7 \cdot 2^{3j}}{N_p} \right\}, \quad (14)$$

where the influence of the Poisson noise has been removed. The asymmetry of the PDF of $n_j(\mathbf{x})$ can be quantified by its skewness defined as

$$S[n_j] = \frac{M_3[n_j]}{(M_2[n_j])^{3/2}}. \quad (15)$$

The scale-dependent flatness, which measures the intermittency at scale 2^{-j} , is defined by

$$F[n_j] = \frac{M_4[n_j]}{(M_2[n_j])^2}. \quad (16)$$

For a Gaussian distribution, the flatness equals three at all scales. In Ref. [44], it was shown that the flatness is directly related to the energy spectrum of Eq. (12) and the standard deviation of the spatial variability of $E[n_j] = M_2[n_j]/\Delta k_j$,

$$F[n_j] = \left(\frac{\vartheta[n_j]}{M_2[n_j]} \right)^2 + 1, \quad (17)$$

where $\vartheta[n_j]$ is the standard deviation and defined as $\vartheta[n_j] = \sqrt{M_4[n_j] - (M_2[n_j])^2}$. This relation explains that intermittency can be quantified by scale-dependent flatness. The influence of the Poisson noise on $M_3[n_j]$ and $M_4[n_j]$ is briefly discussed in Appendix A. This influence cannot be removed only by subtracting the moments for randomly distributed particles. Thus, we use the conventional definition of Eqs. (15) and (16). Note that the particle number dependence of skewness and flatness is assessed in Appendix B.

IV. NUMERICAL RESULTS

A. Scale-dependence of particle clusters and voids

Figure 1 presents wavelet spectra of number density fluctuations $E[n_j]$ together with number density Fourier spectra $E_n(k)$ at different Stokes numbers. The wave numbers k_j and k are normalized by the Kolmogorov scale η . The time-averaged values obtained from particle position data at ten time instants are plotted. The error bars for $E[n_j]$ indicate plus-minus one standard deviation of the wavelet energy spectrum for ten time instants. In Fig. 1, we can see that when $St \leq 1.0$, the spectra $E[n_j]$ increase with St for each $k_j\eta$, having a peak at $k_j\eta \approx 0.2$. This increase suggests that the particle clustering becomes prominent as St becomes larger. In the case that $St \geq 1.0$, at larger scales $k_j\eta \lesssim 10^{-1}$, the spectra become larger with St . In contrast, at scales satisfying $k_j\eta \gtrsim 10^{-1}$, the spectra become smaller for each $k_j\eta$, as St increases from unity. This nonmonotonic behavior of $E[n_j]$ in terms of St shows that the scale of the most intense particle clustering becomes larger with $St (\geq 1.0)$. The St dependence of $E[n_j]$ is in accordance with that reported by Ref. [3]. We can also see that for each St , $E[n_j]$ is in good agreement with the number density Fourier spectra $E_n(k)$. It should be noted that a number density Fourier spectrum could contain the Poisson noise caused by the discrete nature of particle distribution when the standard Fourier transform is applied to the number density field [61]. In the Fourier spectra in Fig. 1, the Poisson noise is removed by using the analytical Fourier transform technique of Ref. [3].

As explained in Sec. III B, the noise is also removed in the wavelet spectra. The wavelet spectra $E[n_j]$ based on Eq. (12) are plotted for the case of random particle positions with uniform probability as reference. Similarly to the inertial particle cases, the average for ten realizations is taken. We confirmed that $E[n_j]$ for the randomly distributed particles agrees with the analytical estimate $E[n_j] = M_{2,\text{random}}[n_j]/\Delta k_j$. As shown in Fig. 1, the influence of the noise can be comparable to

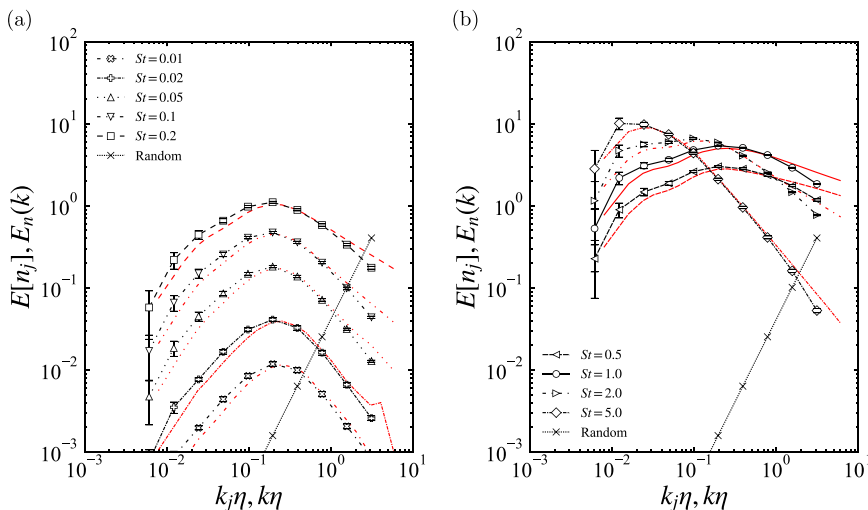


FIG. 1. Wavelet spectra $E[n_j]$ (black) and Fourier spectra $E_n(k)$ (red) of number density fluctuation at $\text{Re}_\lambda = 204$ for the cases of (a) $\text{St} \leq 0.2$ and (b) $\text{St} \geq 0.5$. The error bars for $E[n_j]$ indicate plus-minus one standard deviation obtained from particle position data at ten time instants.

or larger than the wavelet spectra. In this paper, we use the ratio of the energy spectrum $E[n_j]$ for inertial particles to that for randomly distributed particles as the signal/noise ratio (SNR); i.e., $\text{SNR} = E[n_j] \Delta k_j / M_{2,\text{random}}[n_j]$. The effect of the Poisson noise on the statistics is negligibly small when SNR is larger than 10, and otherwise the statistics are contaminated by the Poisson noise (see also Appendix B).

To get intuitive ideas about particle clustering and its scale dependence, we visualize spatial distributions of scale-dependent number density fields n_j in a two-dimensional plane at different scales for $\text{St} = 1.0$ and $\text{St} = 0.05$ together with the total number density fields $n(\mathbf{x})$ in Fig. 2 for $\text{Re}_\lambda = 204$. The scale-dependent number density field n_j is normalized by $\sigma[n_j]$, the standard deviation of n_j . Here, $\sigma[n_j] = \sqrt{M_2[n_j]}$. In Figs. 2(a) and 2(b), we can see the prominence of the particle clusters and void regions, especially at $\text{St} = 1.0$. The prominence of the clusters becomes substantial as scales become smaller, i.e., the scale index j increases. In addition, it seems that the clusters and the voids are distributed more intermittently in space with increasing j for each St . At the scale $j = 8$ ($k_8 \eta = 1.6$) for $\text{St} = 0.05$, the SNR is smaller than 1, which means that the spatial fluctuation of n_j in Fig. 2(h) is mostly due to the Poisson noise.

B. Reynolds number dependence

We examine the influence of the Reynolds number Re_λ on the scale-dependent skewness and flatness values, $S[n_j]$ and $F[n_j]$. The DNS for the three Reynolds numbers, Re_λ , uses different number of particles (imposed by their computational cost), as shown in Table I. Thus, we also consider three sets of randomly distributed particles with the corresponding number of particles. Figure 3 shows that for $\text{St} = 1.0$ the skewness $S[n_j]$ and flatness $F[n_j]$ increase with $k_j \eta$, irrespective of the values of Re_λ . Similarly to Fig. 1, the time-averaged values of $S[n_j]$ and $F[n_j]$ for the data at ten time instants are plotted, together with the error bars indicating plus-minus one standard deviation of $S[n_j]$ or $F[n_j]$ calculated from the data at ten time instants. In Fig. 3(a), we can see that the skewness values $S[n_j]$ for three Re_λ well collapse in the range $0.02 \lesssim k_j \eta \lesssim 0.2$, which suggests the Re_λ dependence of $S[n_j]$ is negligible in this $k_j \eta$ range. In contrast, Fig. 3(b) shows that $F[n_j]$ increases weakly with Re_λ for fixed $k_j \eta$ in the same range. We note that the increase is small in the

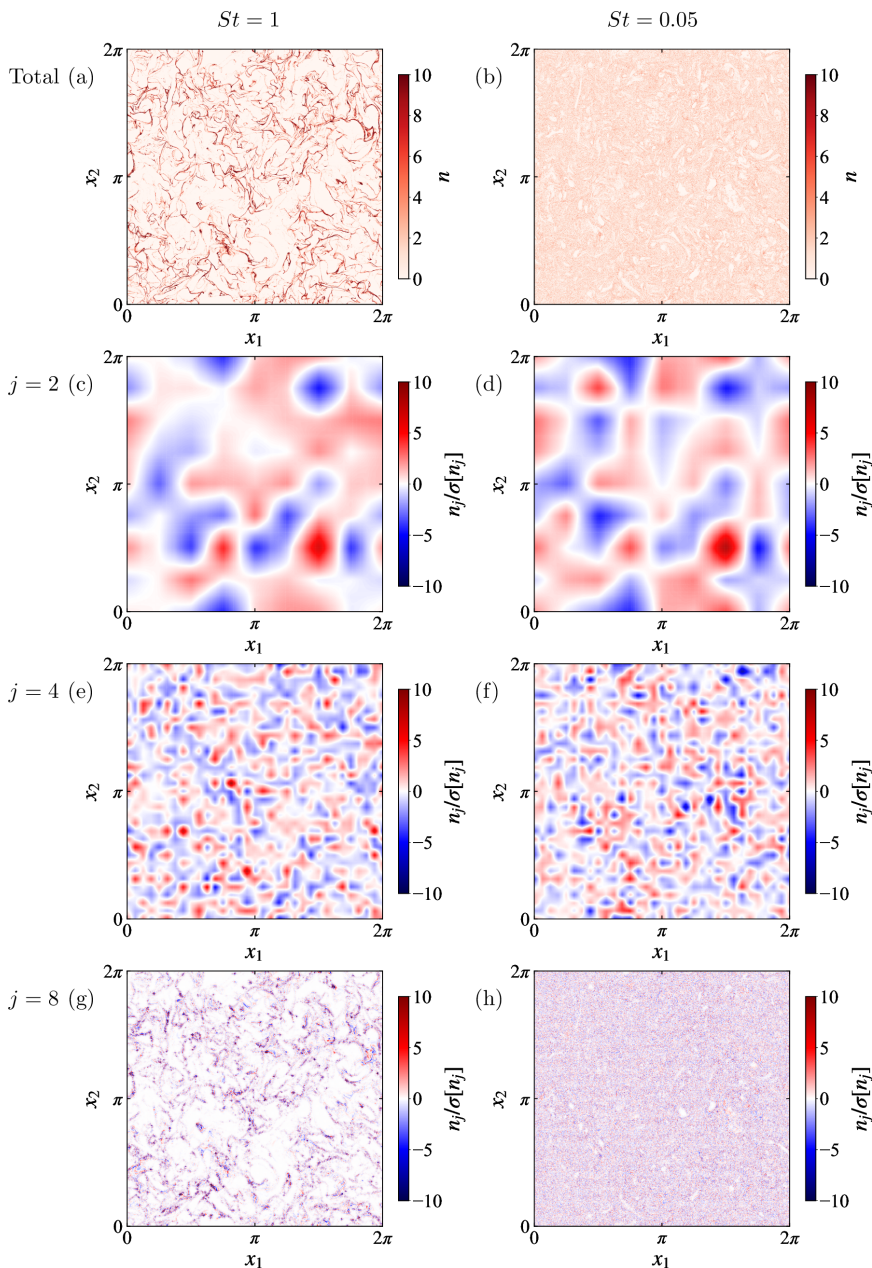


FIG. 2. Spatial distributions of total number density field $n(\mathbf{x})$ (a, b) and scale contributions $n_j(\mathbf{x})$ at $j = 2$ ($k_2\eta = 2.4 \times 10^{-2}$) (c, d), $j = 4$ ($k_4\eta = 9.7 \times 10^{-2}$) (e, f), and $j = 8$ ($k_8\eta = 1.6$) (g, h) in a x_1 - x_2 cross section; (a, c, e, g) $St = 1.0$, (b, d, f, h) $St = 0.05$ for $Re_\lambda = 204$.

figure but sufficiently larger than the standard deviation shown by the error bar. It is conjectured that the scale-dependent particle density field in this range becomes more intermittent with increasing Re_λ .

Note that the statistics of the particle-number density field for randomly distributed particles are equivalent to those for fluid particles ($St = 0$). The number density of the fluid particles is

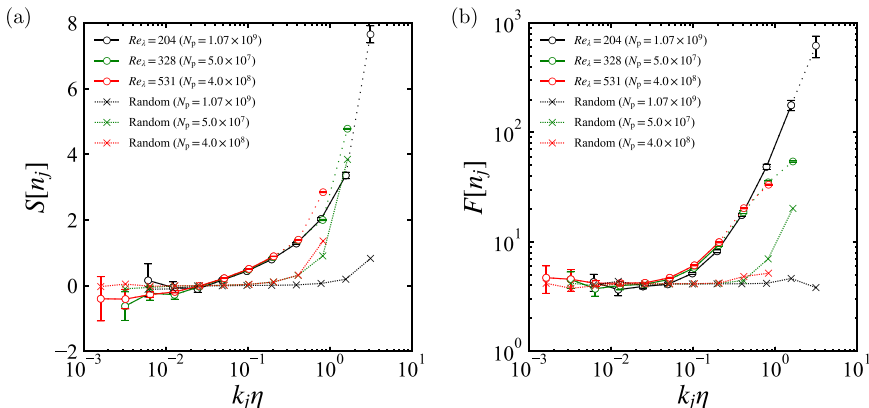


FIG. 3. Reynolds number dependence of scale-dependent skewness $S[n_j]$ and flatness $F[n_j]$ for $St = 1.0$. For $St = 1.0$, solid lines connect the symbols for the scales for which $SNR \geq 10$, and dotted lines are used otherwise. The error bars indicate plus-minus one standard deviation from particle position data at ten time instants.

uniform due to the volume-preserving nature of the incompressible flow. Thus, void and cluster regions are absent. For the case of randomly distributed particles, the skewness values vanish and flatness values remain constant if the number of particles N_p is sufficiently large. The deviation of the skewness and flatness values for the randomly distributed particles in Fig. 3 is mainly due to the finite numbers of particles N_p . It is confirmed in Appendix B that, for the case of inertial particles, the N_p dependence due to the Poisson noise is negligibly small for $S[n_j]$ and $F[n_j]$ at scales where $SNR \geq 10$. Thus, in Fig. 3, the skewness and flatness values for $St = 1.0$ are connected by solid lines at scales where $SNR \geq 10$ and dotted lines are used otherwise. For $Re_\lambda = 204$, $S[n_j]$ and $F[n_j]$ are nearly independent of N_p for $k_j \eta \lesssim 2$. For the higher Reynolds number cases, as illustrated by the dotted lines, the N_p dependence of $S[n_j]$ and $F[n_j]$ is not quantitatively negligible for $k_j \eta \gtrsim 0.2$. Thus, here we limit the discussion of the Re_λ dependence only to the range $k_j \eta \lesssim 0.2$.

C. Stokes number dependence

The Stokes number dependence of $F[n_j]$ and $S[n_j]$ is assessed. Figure 4 shows the scale-dependent flatness $F[n_j]$ for different Stokes numbers. Similar to Fig. 3, the values for inertial particles are connected by solid lines at scales where $SNR \geq 10$ and dotted lines are used otherwise. For the case of $0.5 \leq St \leq 2.0$, $F[n_j]$ increases as the scale becomes smaller, showing that intermittency of clustering is significant in small scales. For $St = 5.0$, $F[n_j]$ is smaller than that of $St = 2.0$ for $k_j \eta \gtrsim 0.3$; i.e., clusters are less intermittently distributed at small scales. This observation for $St = 5.0$ is attributed to weak sensitivity of the particles to small eddies. The most interesting point in this result is that, for $St \leq 0.2$, the flatness $F[n_j]$ at intermediate scales ($0.02 \lesssim k_j \eta \lesssim 0.4$) increases as the Stokes number decreases. One might think that this result is in contradiction to the intuition that the inertial particle distribution becomes close to a random distribution as the Stokes number decreases. However, we should note that this is not due to the lack of statistical samples because the standard deviation, which represents the statistical error, is sufficiently small compared with the difference of $F[n_j]$ from the random case. In addition, as discussed in Appendix B, both the N_g dependence and N_p dependence are negligibly small at these scales.

Bassenne *et al.* [53] also applied wavelet analysis to their DNS data for $St = 0.1, 1$ and 10 at $Re_\lambda = 81$. Note that they used a different forcing scheme and the definitions of the characteristic scales slightly differ. They evaluated the flatness of the local wavelet energy spectra $F[E_{j,i}]$, where

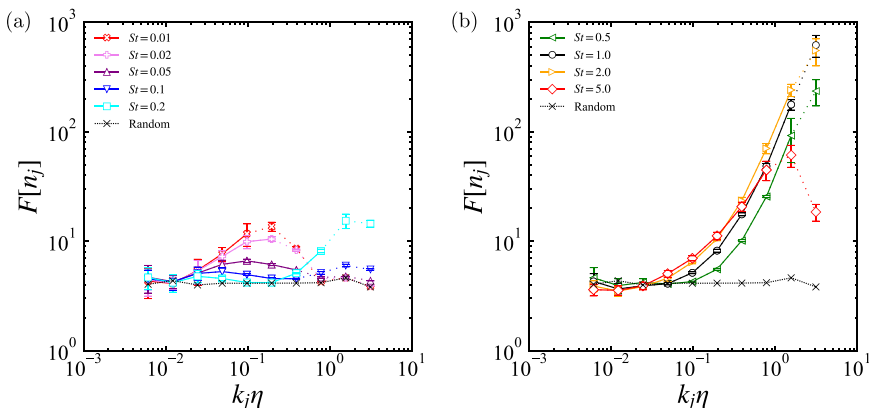


FIG. 4. Scale-dependent flatness $F[n_j]$ at $Re_\lambda = 204$ for (a) $St \leq 0.2$ and (b) $St \geq 0.5$. Solid lines connect the symbols at the scales for which $SNR \geq 10$, and dotted lines are used otherwise. The error bars indicate plus-minus one standard deviation obtained from particle position data at ten time instants.

$E_{j,i} = (N_g^3 2^{-3j} / \Delta k_j) \sum_{\mu=1}^7 (\tilde{n}_{\mu,\gamma})^2$, (i.e., eighth-order scale-dependent statistics) to quantify the intermittency of particle clustering. Their statistics are not equivalent to $F[n_j]$ but the St dependence in their results (Fig. 7 in Ref. [53]) is qualitatively similar to our results: i.e., in Ref. [53], the flatness for $St = 0.1$ is larger than that for $St = 1$ at $0.02 \lesssim k_j \eta \lesssim 0.1$, whereas the flatness for $St = 1$ is close to that for random particles in the same wave-number range. Since Fig. 4(a) contains $F[n_j]$ for smaller St , we can conclude that for $0.01 \leq St \leq 0.2$ the intermittency of particle clustering at the intermediate scales increases when decreasing St .

Figure 5 shows the scale-dependent skewness $S[n_j]$ for different Stokes numbers. For the cases of $0.5 \leq St \leq 2.0$, $S[n_j]$ increases as the scale becomes smaller, and, for $St = 5.0$, the increase with $k_j \eta$ is weaker. For $St \leq 0.2$, the skewness $S[n_j]$ shows negative values at intermediate scales ($0.02 \lesssim k_j \eta \lesssim 0.4$). For these intermediate scales, we observe that for $St \leq 0.2$ the skewness locally has a concave shape, corresponding in the flatness to a locally convex shape. The local minima of skewness values and the local maxima of the flatness occur at similar scales. Physical insights of the negative skewness are given in Sec. IV D.

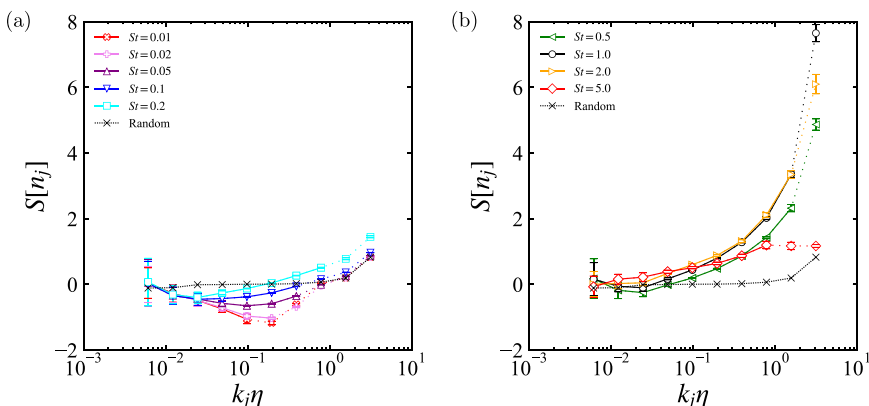


FIG. 5. Scale-dependent skewness $S[n_j]$ at $Re_\lambda = 204$ for (a) $St \leq 0.2$ and (b) $St \geq 0.5$. Solid lines connect the symbols at the scales for which $SNR \geq 10$, and dotted lines are used otherwise. The error bars indicate plus-minus one standard deviation obtained from particle position data at 10 time instants.

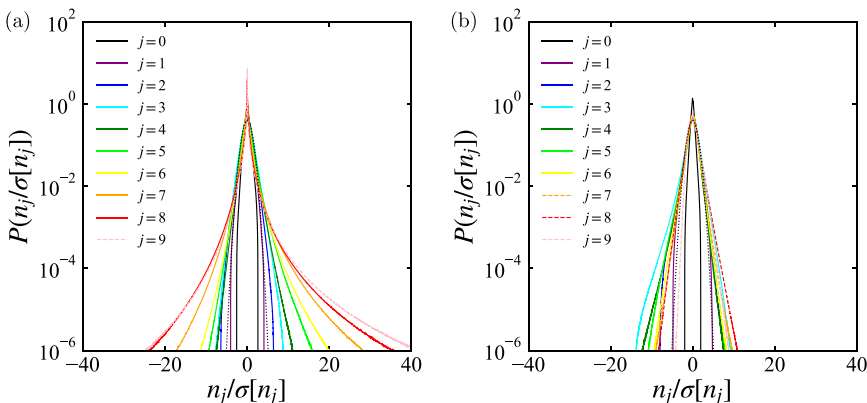


FIG. 6. PDF of the normalized scale-dependent particle number density $n_j/\sigma[n_j]$ for (a) $St = 1.0$ and (b) $St = 0.05$ at $Re_\lambda = 204$. Solid lines are used for the scales for which $SNR \geq 10$, and dashed lines for the scales for which $SNR < 10$. The dotted lines correspond to the Gaussian distribution $\mathcal{N}(0, 1)$.

The St dependence of $S[n_j]$ and $F[n_j]$ in the limit of $St \rightarrow 0$ would be of interest to the readers. It is conjectured that when we neglect the effect of Poisson noise, the scale contribution of the number density n_j becomes zero as St decreases to zero. Thus, we expect that the second-, third-, and fourth-order moments (i.e., $M_2[n_j]$, $M_3[n_j]$, and $M_4[n_j]$) also become zero for $St \rightarrow 0$. This means that the $S[n_j]$ and $F[n_j]$ values in the limit of $St \rightarrow 0$ can be indefinite due to the definition in Eqs. (15) and (16). This suggests that the increase of the absolute values of $S[n_j]$ and $F[n_j]$ can be observed when St decreases. When we consider a finite number of particles, the variance of n_j due to the inertial effect would become smaller than the variance due to the Poisson noise for sufficiently small St because $M_{2,\text{random}}[n_j]$ does not depend on St . When the variance of n_j is smaller than the variance due to the Poisson noise, the $S[n_j]$ and $F[n_j]$ values would become close to the values for randomly distributed particles. This trend can be observed in Figs. 4(a) and 5(a) for large wave numbers where $SNR < 10$.

D. Cluster-pronounced and void-pronounced structures

To give a physical interpretation to the St dependence of the skewness and flatness, the PDFs of $n_j(\mathbf{x})$ normalized by the standard deviation $\sigma[n_j]$ for $St = 1.0$ and $St = 0.05$ are shown in Fig. 6. For $St = 1.0$, skewness $S[n_j]$ is positive for $k_j\eta \gtrsim 0.05$ ($j = 4, \dots, 9$) as shown in Fig. 5(a). The PDFs in Fig. 6(a) have heavier tails on the positive side for each j ($j = 4, \dots, 9$). In contrast, for $St = 0.05$, the PDFs in Fig. 6(b) have heavier tails on the negative side for each j ($j = 2, \dots, 6$), where $S[n_j]$ is negative (i.e., $0.02 \lesssim k_j\eta \lesssim 0.4$) as shown in Fig. 5(a). These trends in the PDFs imply that $n_j(\mathbf{x})$ has higher probability of large positive values when $S[n_j] > 0$, while $n_j(\mathbf{x})$ has higher probability of large negative values when $S[n_j] < 0$. Thus, the spatial distribution of $n_j(\mathbf{x})$ is expected to behave like in the schematic figures shown in Fig. 7, and $S[n_j] > 0$ and $S[n_j] < 0$ would suggest cluster-pronounced and void-pronounced structures, respectively. To clarify whether negative skewness is a sign of void-pronounced structures, we verify the relationship between the large negative values of $n_j(\mathbf{x})$ and void regions. Figures 8(a) and 8(b), respectively, show magnified views of Figs. 2(b) and 2(f), which are the total number density $n(\mathbf{x})$ and the scale contribution for $j = 4$, corresponding to $k_4\eta = 9.7 \times 10^{-2}$. Note that the scale index $j = 4$ corresponds to the scale at which the skewness value is minimum at this Stokes number, $St = 0.05$. Figure 8 shows that the location of large negative values in $n_j(\mathbf{x})$ corresponds to void regions in $n(\mathbf{x})$. We can therefore conclude that for $St \leq 0.2$, negative skewness values are indeed indicators for void-pronounced structures.

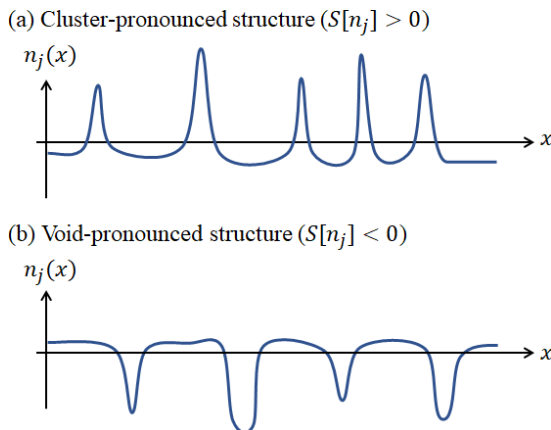


FIG. 7. Schematic figures of (a) cluster- and (b) void-pronounced structures for n_j .

For $0.01 \leq St \leq 0.2$, the scales of local minima of the negative skewness in Fig. 5(a) almost correspond to the scales of local maxima of the flatness in Fig. 4(a). This suggests that the flatness at intermediate scales for $0.01 \leq St \leq 0.2$ is attributed to the intermittent distribution of void regions. It should also be noted that Figs. 5(a) and 4(a) show negative $S[n_j]$ and positive $F[n_j]$ for $St \leq 0.1$ at the scale $k_j \eta \approx 0.2$, which corresponds to the peak location of the energy spectra $E[n_j]$. Thus, the intermittent void distributions play an important role for inertial particle clustering for $0.01 \leq St \leq 0.1$.

The physical mechanism of the intermittent void distributions can be explained by the idea of the local Stokes number [20,62], which was introduced to discuss the effect of intermittency of turbulence on particle collision. Dallas and Vassilicos [62] defined the local Stokes number in two-dimensional turbulence as $St^* \equiv \tau_p \sqrt{2s_{ij}s_{ji}}$, where s_{ij} is the strain-rate tensor, and Onishi and Vassilicos [20] applied that to 3D turbulence. The above local Stokes number was defined to discuss particle collision in cluster regions. To discuss void formation, we define the local Stokes number here using the local enstrophy $\Omega = |\boldsymbol{\omega}|^2/2$ as $St^* \equiv \tau_p \sqrt{2\Omega}$, where $\boldsymbol{\omega} \equiv \nabla \times \mathbf{u}$. Particles with the relaxation time τ_p are sensitive to a vortex with timescale of $\tau_f \sim 1/\sqrt{2\Omega}$ when τ_p is comparable to τ_f , i.e., $St^* \sim 1$. In other words, particles are hardly affected by the vortex when $St^* \ll 1$ or $St^* \gg 1$. For small Stokes number particles, most vortices have τ_f much larger than τ_p but strong vortices have τ_f comparable to τ_p . Such strong vortices are distributed intermittently due to the intermittent nature of turbulence. Thus, the void regions are generated only by these strong vortices and are

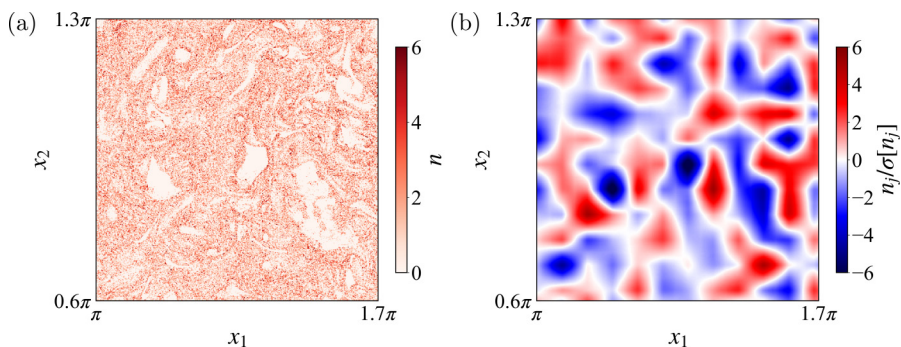


FIG. 8. Magnified spatial distributions of (a) total number density $n(\mathbf{x})$ and (b) scale contributions $n_j(\mathbf{x})$ at $j = 4$ ($k_4 \eta = 9.7 \times 10^{-2}$) for $St = 0.05$ in the same x_1 - x_2 cross section as Fig. 2.

likewise distributed intermittently. As the Stokes number decreases, the number of vortices that satisfy $St^* \sim 1$ decreases and that results in the increase of the absolute values of $S[n_j]$ and $F[n_j]$. Sakurai and Ishihara [63] reported that the width of low-density regions in conditional averaged number density fields in large enstrophy regions is approximately 10η for $St = 0.1$, and this scale is approximately the same as the diameter of vortex tubes. This scale agrees with the scale of negative $S[n_j]$ values for $St \leq 0.05$. They also showed that the width of low-density regions increases as St increases, but it remains smaller than 20η for $St \leq 1$. This fact suggests that the increase of $S[n_j]$ at $k_j\eta \gtrsim 0.1$ for $0.1 \leq St \leq 1.0$ is not due to the increase of the void size but rather due to the increase of the prominence of small-scale clusters. That is, as St increases ($St \leq 1.0$), the void size increases and clusters are confined in a lower-dimensional manifold in space, forming fractal structures thinner than η . Since clusters compensate for the mass loss in the void regions, the clusters become more pronounced than void regions.

Negative skewness values can also be observed in Fig. 3: For $Re_\lambda \geq 328$, $S[n_j]$ shows negative values at large scales $k_j\eta \lesssim 0.02$. Note that the absolute values of $S[n_j]$ in $0.003 \lesssim k_j\eta \lesssim 0.01$ for $Re_\lambda = 531$ are larger than the error bars. It is conjectured that even for $St \sim 1$, void regions are pronounced at large scales, while clusters are pronounced at small scales. This result could be connected to “cloud voids” reported by Karpińska *et al.* [64]. They observed many void regions with the diameter of up to 12 cm during mountain observations and explained that the phenomenon is caused by the inertial motion of cloud particles.

V. CONCLUSION

We have studied scale-dependent statistics of the particle distribution to get insight into the nonuniform and intermittent distribution of inertial particles, i.e., clusters and voids, in isotropic turbulence at high Reynolds number. To this end, orthogonal wavelet analyses have been applied to particle data obtained by performing 3D DNS of particle-laden homogeneous isotropic turbulence for $204 \leq Re_\lambda \leq 531$, using up to 10^9 particles for $0.01 \leq St \leq 5.0$. The number density fields $n(\mathbf{x}, t)$ are obtained by the histogram method using equidistant bins and are then decomposed into scale-dependent contributions $n_j(\mathbf{x}, t)$ at scale 2^{-j} using orthogonal wavelet filtering. Scale-dependent skewness and flatness values have been investigated and the influence of the Reynolds and Stokes number has been assessed. We have also evaluated the wavelet energy spectra $E[n_j]$ for inertial particles, in which the influence of the Poisson noise is removed. We defined the SNR as the ratio of $E[n_j]$ for inertial particles to that for the Poisson noise and discussed the scale-dependent skewness and flatness values at scales where SNR is larger than 10. The following conclusions can be drawn.

We observed that the scale-dependent skewness and flatness values, $S[n_j]$ and $F[n_j]$, are significantly influenced by the Stokes number St . For $0.5 \leq St \leq 2.0$, both the skewness and flatness values become larger, when the scale decreases. This suggests intermittent cluster distribution at small scales. The intermittency is reflected by the increasing flatness values, while the cluster distribution can be explained by the increasing skewness values.

We also found that for small Stokes numbers, $0.01 \leq St \leq 0.2$, the skewness $S[n_j]$ exhibits negative values at intermediate scales, i.e., for scales larger than the Kolmogorov scale and smaller than the integral scale of the flow, and the flatness $F[n_j]$ at the intermediate scales increases as St decreases. We have shown that negative values of $S[n_j]$ imply higher probability of large negative values of n_j . Our visualizations show that these large negative values of n_j can be attributed to void regions of the particle-number density. Hence we can conclude that void regions at the intermediate scales are pronounced and intermittently distributed for $0.01 \leq St \leq 0.2$. The range of negative $S[n_j]$ and positive $F[n_j]$ for $0.01 \leq St \leq 0.1$ includes the scale of the peak of the energy spectra $E[n_j]$. Thus, we conjecture that intermittent void distributions play an important role for inertial particle clustering for $0.01 \leq St \leq 0.1$ for $Re_\lambda = 204$. Our results for higher Reynolds numbers, i.e., for $Re_\lambda = 328$ and 531 , confirm that negative values of the skewness $S[n_j]$ are likewise observed at large scales for $St = 1.0$. This suggests that even for $St \sim 1$, void regions are pronounced at large

scales, while clusters are pronounced at small scales. We also found that for $St = 1.0$, the flatness $F[n_j]$ increases weakly as Re_λ increases at scales larger than the Kolmogorov scale, while the Re_λ dependence of the skewness $S[n_j]$ is negligibly small. These results suggest that the scale-dependent particle density field in these scales becomes more intermittent with increasing Re_λ .

The dynamics of scale-dependent cluster and void formation at scales larger than the Kolmogorov scale is still an open issue and its clarification is of importance for modeling inertial particle clustering in high Reynolds number turbulence. The present results could contribute to improve the empirical model for the Fourier spectrum [3,4] and the analytical estimates [31,36] of multiscale inertial clustering, which are based on the assumption of Gaussianity. The divergence of the particle velocity also plays a key role, as recently shown in Ref. [65]. Analyzing the dynamics of the scale-dependent divergence is an interesting perspective for future work.

ACKNOWLEDGMENTS

K.M. acknowledges financial support from Grant-in-Aid for Young Scientists (B) No. JP17K14598 and Scientific Research (C) No. JP20K04298 from the Japan Society for the Promotion of Science (JSPS). He is also grateful to I2M for kind hospitality during his stay at Aix-Marseille Université. K.Y. acknowledges financial support from Grant-in-Aid for Scientific Research (S) No. JP16H06339 from the JSPS, and thanks I2M for kind hospitality during his stay at Aix-Marseille Université. K.S. acknowledges kind hospitality during his visit at JAMSTEC and financial support. The DNSs presented here were conducted on the Earth Simulator supercomputer system operated by JAMSTEC.

APPENDIX A: ANALYTICAL ESTIMATES FOR POISSON NOISE

1. Second-order moment

To obtain an analytical estimate of the second-order scale-dependent moment for Poisson noise, we first explain the contribution of the Poisson noise in the correlation function of the particle distribution. To this end, we consider the spatial correlation function for $n_\delta(\mathbf{x}, t)$ of Eq. (6), defined as

$$\begin{aligned} \Phi_\delta(\mathbf{r}) &\equiv \langle n_\delta(\mathbf{x} + \mathbf{r})n_\delta(\mathbf{x}) \rangle \\ &= \left\langle (2\pi)^{-3} \int_{\mathbb{T}^3} n_\delta(\mathbf{x} + \mathbf{r})n_\delta(\mathbf{x})d\mathbf{x} \right\rangle. \end{aligned} \quad (\text{A1})$$

As mentioned in Ref. [4], the spatial correlation function $\Phi_\delta(\mathbf{r})$ is discontinuous at $\mathbf{r} = \mathbf{0}$ because the particle distribution is composed of spatially discrete points. The discontinuity is explained by decomposing the correlation as follows: Substituting Eq. (6) into Eq. (A1) results in

$$\Phi_\delta(\mathbf{r}) = \frac{1}{n_0^2} \left\langle \sum_{m=1}^{N_p} \delta(\mathbf{x} + \mathbf{r} - \mathbf{x}_{p,m})\delta(\mathbf{x} - \mathbf{x}_{p,m}) \right\rangle + \frac{1}{n_0^2} \left\langle \sum_{m=1}^{N_p} \delta(\mathbf{x} + \mathbf{r} - \mathbf{x}_{p,m}) \sum_{m'=1, m' \neq m}^{N_p} \delta(\mathbf{x} - \mathbf{x}_{p,m'}) \right\rangle. \quad (\text{A2})$$

The first term represents the correlation of identical particle positions and the second term represents the correlation between different particles. When we consider the discrete particle distribution as a stochastic realization in a certain probability density field, the second term corresponds to the correlation of the probability density field. Thus, the second term does not depend on the number of particles. On the other hand, the first term appears only for the case of discrete particle distributions. For the case of randomly distributed particles with uniform probability, the second term becomes a constant, $\langle n \rangle^2$. Therefore, the first term can be considered as the Poisson noise contribution. By

applying spatial averaging (integration with respect to \mathbf{x}) to the first term, we obtain

$$\Phi_\delta(\mathbf{r}) = \frac{1}{n_0} \delta(\mathbf{r}) + \Phi(\mathbf{r}), \quad (\text{A3})$$

where $\Phi(\mathbf{r})$ is the spatial correlation function of the probability density field. Similar arguments to Eq. (A3) are also given in Refs. [4,61].

When we apply the wavelet transform, the number-density field data on equidistant grid points are obtained based on the histogram method as described by Eq. (7). To account for the contribution of the histogram method, we consider the spatial correlation function for $n(\mathbf{x})$, defined as $\Phi_K(\mathbf{r}) \equiv \langle n(\mathbf{x} + \mathbf{r})n(\mathbf{x}) \rangle$. By using the continuous definition of $n(\mathbf{x})$, i.e., $n(\mathbf{x}) = \int_{\mathbb{T}^3} K_h(\mathbf{x} - \mathbf{x}')n_\delta(\mathbf{x}')d\mathbf{x}'$, $\Phi_K(\mathbf{r})$ is given by

$$\Phi_K(\mathbf{r}) = \frac{1}{n_0} K_h^2(\mathbf{r}) + \int_{\mathbb{T}^3} K_h^2(\mathbf{r} - \mathbf{r}')\Phi(\mathbf{r}')d\mathbf{r}', \quad (\text{A4})$$

where $K_h^2(\mathbf{x})$ is defined as $K_h^2(\mathbf{x}) = \int_{\mathbb{T}^3} K_h(\mathbf{x} - \mathbf{x}')K_h(\mathbf{x}')d\mathbf{x}'$ and where $K_h(\mathbf{x})$ is a kernel function, corresponding in the current case of the histogram to a piecewise constant function (see also Sec. II C).

Using the spatial correlation function $\Phi_K(\mathbf{r})$, we evaluate the contribution of the Poisson noise for the second-order moment $M_2[n_j]$. Due to the orthogonality of wavelets, $M_2[n_j]$ is given by

$$M_2[n_j] = \sum_{\mu=1}^7 \sum_{i_1, i_2, i_3=0}^{2^j-1} (\tilde{n}_{\mu, \gamma})^2. \quad (\text{A5})$$

Inserting the L^2 inner product of $\tilde{n}_{\mu, \gamma} = \langle n, \psi_{\mu, \gamma} \rangle$, we obtain

$$M_2[n_j] = (2\pi)^{-6} \sum_{\mu=1}^7 \sum_{i_1, i_2, i_3=0}^{2^j-1} \int_{\mathbb{T}^3} \int_{\mathbb{T}^3} n(\mathbf{x} + \mathbf{r})n(\mathbf{x})\psi_{\mu, \gamma}(\mathbf{x} + \mathbf{r})\psi_{\mu, \gamma}(\mathbf{x})d\mathbf{r}d\mathbf{x}. \quad (\text{A6})$$

In Eq. (A6), $\sum_{i_1, i_2, i_3=0}^{2^j-1} \psi_{\mu, \gamma}(\mathbf{x} + \mathbf{r})\psi_{\mu, \gamma}(\mathbf{x})$ is for fixed \mathbf{r} a $2\pi/2^j$ periodic oscillating function for \mathbf{x} over the space of \mathbb{T}^3 , and it is statistically uncorrelated with $n(\mathbf{x} + \mathbf{r})n(\mathbf{x})$. Thus, when the sample number 2^{3j} is sufficiently large, $M_2[n_j]$ is approximately given by

$$M_2[n_j] \approx (2\pi)^{-3} 2^{3j} \sum_{\mu=1}^7 \int_{\mathbb{T}^3} \Phi_K(\mathbf{r})\Psi_{\mu, j}^2(\mathbf{r})d\mathbf{r}, \quad (\text{A7})$$

where $\Psi_{\mu, j}^2(\mathbf{r})$ is the spatial correlation function of the wavelet and defined as $\Psi_{\mu, j}^2(\mathbf{r}) \equiv (2\pi)^{-3} \int_{\mathbb{T}^3} \psi_{\mu, \gamma}(\mathbf{x} + \mathbf{r})\psi_{\mu, \gamma}(\mathbf{x})d\mathbf{x}$. Note that $\Psi_{\mu, j}^2(\mathbf{r})$ is independent of the translation of wavelets. Substitution of Eq. (A4) into Eq. (A7) yields

$$M_2[n_j] = \frac{2^{3j}}{N_p} \sum_{\mu=1}^7 \int_{\mathbb{T}^3} K_h^2(\mathbf{r})\Psi_{\mu, j}^2(\mathbf{r})d\mathbf{r} + (2\pi)^{-3} 2^{3j} \sum_{\mu=1}^7 \int_{\mathbb{T}^3} \int_{\mathbb{T}^3} K_h^2(\mathbf{r} - \mathbf{r}')\Phi(\mathbf{r}')d\mathbf{r}'\Psi_{\mu, j}^2(\mathbf{r})d\mathbf{r}, \quad (\text{A8})$$

where the first term is the contribution of the Poisson noise and the second term is the statistics of the probability density field. To estimate the contribution of the Poisson noise accurately, we consider the discrete form of the integral $\int_{\mathbb{T}^3} K_h^2(\mathbf{r})\Psi_{\mu, j}^2(\mathbf{r})d\mathbf{r}$, using the trapezoidal rule $\sum_{i_1, i_2, i_3=0}^{N_g-1} h^3 K_h^2(\mathbf{r}_{i_1, i_2, i_3})\Psi_{\mu, j}^2(\mathbf{r}_{i_1, i_2, i_3})$ with $h = 2\pi/N_g$. Since $K_h^2(x_{i_1, i_2, i_3})$ is in the current case zero except at the point $i_1 = i_2 = i_3 = 0$, it yields $\int_{\mathbb{T}^3} K_h^2(\mathbf{r})\Psi_{\mu, j}^2(\mathbf{r})d\mathbf{r} = \Psi_{\mu, j}^2(\mathbf{0}) = \langle \psi_{\mu, \gamma}, \psi_{\mu, \gamma} \rangle = 1$.

In the consequence, we obtain

$$M_2[n_j] = \frac{7 \cdot 2^{3j}}{N_p} + (2\pi)^{-3} 2^{3j} \sum_{\mu=1}^7 \int_{\mathbb{T}^3} \int_{\mathbb{T}^3} K_h^2(\mathbf{r} - \mathbf{r}') \Phi(\mathbf{r}') d\mathbf{r}' \Psi_{\mu,j}^2(\mathbf{r}) d\mathbf{r}. \quad (\text{A9})$$

For the case of randomly distributed particles with uniform probability, the second term vanishes. Thus, the effect of the Poisson noise on $M_2[n_j]$ is given by Eq. (13) and the wavelet energy spectrum after removing the Poisson noise contribution is given by Eq. (14).

Removing the influence of Poisson noise on second-order statistics of the particle distribution has been proposed previously. Similar computations have been done in Refs. [3,61] for the Fourier spectrum and in Ref. [66] to correct the variance of number-density fields obtained by the box-counting method.

2. Higher-order moments

For higher-order moments, the Poisson noise contribution cannot be removed by subtracting the moments for the randomly distributed particles. For example, in the case of the third-order moment, the third-order spatial correlation function for $n_\delta(\mathbf{x})$ is defined as

$$\begin{aligned} \Phi_{\delta,3}(\mathbf{r}_1, \mathbf{r}_2) &\equiv \langle n_\delta(\mathbf{x}) n_\delta(\mathbf{x} + \mathbf{r}_1) n_\delta(\mathbf{x} + \mathbf{r}_2) \rangle \\ &= (2\pi)^{-3} \left\langle \int_{\mathbb{T}^3} n_\delta(\mathbf{x}) n_\delta(\mathbf{x} + \mathbf{r}_1) n_\delta(\mathbf{x} + \mathbf{r}_2) d\mathbf{x} \right\rangle. \end{aligned} \quad (\text{A10})$$

Similar to $\Phi_\delta(\mathbf{r})$, $\Phi_{\delta,3}(\mathbf{r}_1, \mathbf{r}_2)$ is also discontinuous due to the spatial correlation of identical particles. For the case of randomly distributed particles with uniform probability, the discontinuity of $\Phi_{\delta,3}(\mathbf{r}_1, \mathbf{r}_2)$ at $\mathbf{r}_1 = \mathbf{r}_2 = \mathbf{0}$ (i.e., three particles are identical) gives the finite values of $M_3[n_j]$. However, when the probability density field is not uniform, the discontinuity at $\mathbf{r}_1 = \mathbf{0}$ or $\mathbf{r}_2 = \mathbf{0}$ or $\mathbf{r}_1 = \mathbf{r}_2$ (i.e., two of three particles are identical) also results in the particle number dependence of $M_3[n_j]$. Thus, $M_3[n_j]$ without the Poisson noise contribution cannot be obtained only by subtracting $M_3[n_j]$ for randomly distributed particles. Similar arguments hold for higher order moments.

APPENDIX B: GRID NUMBER AND PARTICLE NUMBER DEPENDENCE

The influence of the numerical parameters, i.e., the number of grid points N_g and the number of particles N_p in simulations, can be crucial when performing statistical analyses, especially for higher order statistics. We check the influence of these parameters on the energy spectra $E[n_j]$, scale-dependent skewness $S[n_j]$, and flatness $F[n_j]$ of particle-number density fields $n(\mathbf{x})$ in the DNS for $St = 1.0$ and $Re_\lambda = 204$. In addition, we compare them with randomly distributed particles. Figure 9 quantifies the impact of N_g and N_p on the scale-dependent statistics, $E[n_j]$, $S[n_j]$, and $F[n_j]$, plotted as a function of $k_j \eta$. Figure 9(a) illustrates that doubling N_g from 512 to 1024 has a small influence on the energy spectrum of inertial particles at small scales due to the difference of the filter size for the histogram method in Eq. (7), while the doubling does not impact the spectrum for randomly distributed particles. Changing the number of particles N_p , while keeping the grid size fixed ($N_g = 1024$), shows large impact for randomly distributed particles in Fig. 9(b). We have confirmed that the spectra for randomly distributed particles are consistent with our analytical estimate given by $M_{2,\text{random}}[n_j]/\Delta k_j$. Figure 9(b) further shows that the N_p dependence of the spectra is negligibly small, meaning that the Poisson noise is appropriately removed by Eq. (14).

Figure 9(c) shows that the number of grid points N_g has small impact on $S[n_j]$ only at the smallest scale of each N_g . The influence of N_g becomes even weaker for $F[n_j]$, as shown in Fig. 9(e). For the random cases, we observe that for each N_g , $S[n_j]$ increases only weakly with decreasing scale and $F[n_j]$ even remains almost constant. Thus, the influence of N_g on $S[n_j]$ and $F[n_j]$ is negligibly small (less than 3%) except at the smallest scale. However, as observed in Figs. 9(d) and 9(f), the number of particles N_p has some impact on both $S[n_j]$ and $F[n_j]$. For inertial particles, we

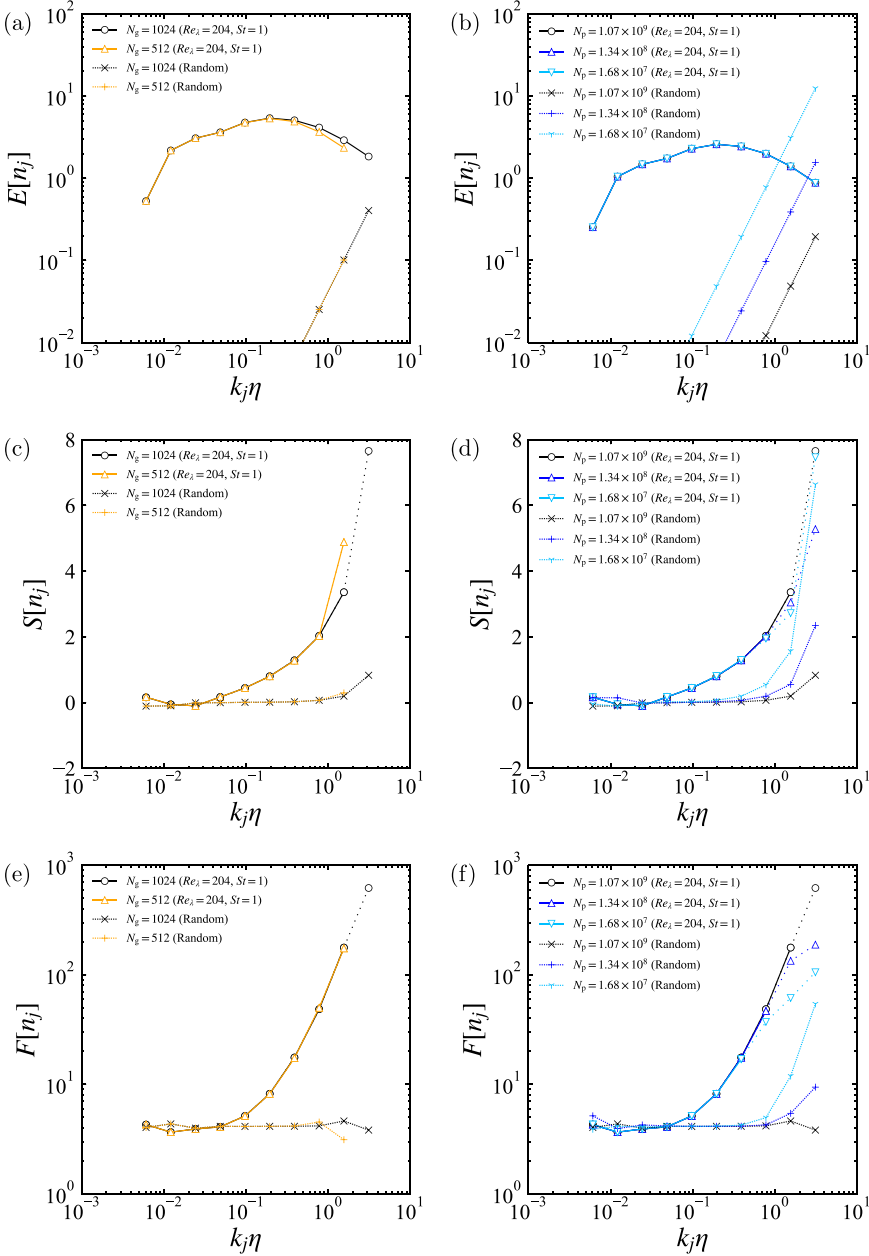


FIG. 9. Wavelet spectra $E[n_j]$ (a, b), scale-dependent skewness $S[n_j]$ (c, d), and scale-dependent flatness $F[n_j]$ (e, f) at $Re_\lambda = 204$ and $St = 1.0$ for (a, c, e) $N_g = 512$ and 1024 at fixed $N_p (= 1.07 \times 10^9)$ and for (b, d, f) $N_p = 1.68 \times 10^7$, 1.34×10^8 and 1.07×10^9 at fixed $N_g (= 1024)$. Dotted lines for $S[n_j]$ and $F[n_j]$ indicate $SNR < 10$.

find that the growth of $S[n_j]$ and $F[n_j]$ with $k_j \eta$ becomes more pronounced when increasing the number of particles from $N_p = 1.68 \times 10^7$ to $N_p = 1.07 \times 10^9$. For the random case, this trend is inverted: Increasing N_p yields more stable statistical estimators and thus the growth of $S[n_j]$ and $F[n_j]$ with $k_j \eta$ is reduced. As for randomly distributed particles, void and cluster regions are

absent, the skewness values should vanish, and the flatness values should remain constant with scale. In other words, deviation of the skewness and flatness values for the random case is caused by statistical sampling, i.e., the finite numbers of particles N_p . The above observations illustrate the importance of using a sufficiently large number of particles to get statistically converged results and to observe skewness and flatness values independent of N_p . The increasing values of $S[n_j]$ and $F[n_j]$ with $k_j\eta$, i.e., for decreasing scale, in the random cases can thus be used to determine whether N_p is sufficiently large or not. In this paper, we introduced the SNR defined by $\text{SNR} = E[n_j]\Delta k_j/M_{2,\text{random}}[n_j]$. For inertial particles $S[n_j]$ and $F[n_j]$ values at scales where $\text{SNR} \geq 10$ are connected by solid lines, while dotted lines are used for $\text{SNR} < 10$, cf. Fig. 9. When we consider only the values for $\text{SNR} \geq 10$, the error due to the N_p dependence is less than 2% for $S[n_j]$ and less than 4% for $F[n_j]$, which means that the N_p dependence is negligibly small.

-
- [1] R. A. Shaw, Particle-turbulence interactions in atmospheric clouds, [Annu. Rev. Fluid Mech. 35, 183 \(2003\)](#).
 - [2] P. J. Ireland, A. D. Bragg, and L. R. Collins, The effect of Reynolds number on inertial particle dynamics in isotropic turbulence. Part 1. Simulations without gravitational effects, [J. Fluid Mech. 796, 617 \(2016\)](#).
 - [3] K. Matsuda, R. Onishi, M. Hirahara, R. Kurose, K. Takahashi, and S. Komori, Influence of microscale turbulent droplet clustering on radar cloud observations, [J. Atmos. Sci. 71, 3569 \(2014\)](#).
 - [4] K. Matsuda and R. Onishi, Turbulent enhancement of radar reflectivity factor for polydisperse cloud droplets, [Atmos. Chem. Phys. 19, 1785 \(2019\)](#).
 - [5] F. Toschi and E. Bodenschatz, Lagrangian properties of particles in turbulence, [Annu. Rev. Fluid Mech. 41, 375 \(2009\)](#).
 - [6] R. Monchaux, M. Bourgoin, and A. Cartellier, Analyzing preferential concentration and clustering of inertial particles in turbulence, [Int. J. Multiphase Flow 40, 1 \(2012\)](#).
 - [7] M. R. Maxey and J. J. Riley, Equation of motion for a small rigid sphere in a nonuniform flow, [Phys. Fluids 26, 883 \(1983\)](#).
 - [8] L.-P. Wang and M. R. Maxey, Settling velocity and concentration distribution of heavy particles in homogeneous isotropic turbulence, [J. Fluid Mech. 256, 27 \(1993\)](#).
 - [9] M. R. Maxey, The gravitational settling of aerosol particles in homogeneous turbulence and random flow fields, [J. Fluid Mech. 174, 441 \(1987\)](#).
 - [10] K. D. Squires and J. K. Eaton, Measurements of particle dispersion obtained from direct numerical simulations of isotropic turbulence, [J. Fluid Mech. 226, 1 \(1991\)](#).
 - [11] S. Sundaram and L. R. Collins, Collision statistics in an isotropic particle-laden turbulent suspension. Part 1. Direct numerical simulations, [J. Fluid Mech. 335, 75 \(1997\)](#).
 - [12] W. C. Reade and L. R. Collins, Effect of preferential concentration on turbulent collision rates, [Phys. Fluids 12, 2530 \(2000\)](#).
 - [13] O. Ayala, B. Rosa, L.-P. Wang, and W. Grabowski, Effects of turbulence on the geometric collision rate of sedimenting droplets. Part 1. Results from direct numerical simulation, [New J. Phys. 10, 075015 \(2008\)](#).
 - [14] O. Ayala, B. Rosa, and L.-P. Wang, Effects of turbulence on the geometric collision rate of sedimenting droplets. Part 2. Theory and parameterization, [New J. Phys. 10, 075016 \(2008\)](#).
 - [15] L. I. Zaichik and V. M. Alipchenkov, Refinement of the probability density function model for preferential concentration of aerosol particles in isotropic turbulence, [Phys. Fluids 19, 113308 \(2007\)](#).
 - [16] L. I. Zaichik and V. M. Alipchenkov, Statistical models for predicting pair dispersion and particle clustering in isotropic turbulence and their applications, [New J. Phys. 11, 103018 \(2009\)](#).
 - [17] R. Onishi, K. Takahashi, and S. Komori, Influence of gravity on collisions of monodispersed droplets in homogeneous isotropic turbulence, [Phys. Fluids 21, 125108 \(2009\)](#).
 - [18] L.-P. Wang, B. Rosa, H. Gao, G. He, and G. Jin, Turbulent collision of inertial particles: Point-particle based, hybrid simulations and beyond, [Int. J. Multiphase Flow 35, 854 \(2009\)](#).

- [19] J. Lu, H. Nordslek, and R. A. Shaw, Clustering of settling charged particles in turbulence: Theory and experiments, *New J. Phys.* **12**, 123030 (2010).
- [20] R. Onishi and J. C. Vassilicos, Collision statistics of inertial particles in two-dimensional homogeneous isotropic turbulence with an inverse cascade, *J. Fluid Mech.* **745**, 279 (2014).
- [21] P. J. Ireland, A. D. Bragg, and L. R. Collins, The effect of Reynolds number on inertial particle dynamics in isotropic turbulence. Part 2. Simulations with gravitational effects, *J. Fluid Mech.* **796**, 659 (2016).
- [22] J. Chun, D. L. Koch, S. L. Rani, A. Ahluwalia, and L. R. Collins, Clustering of aerosol particles in isotropic turbulence, *J. Fluid Mech.* **536**, 219 (2005).
- [23] L.-P. Wang, A. Wexler, and Y. Zhou, Statistical mechanical description and modelling of turbulent collision of inertial particles, *J. Fluid Mech.* **415**, 117 (2000).
- [24] J. Bec, L. Biferale, M. Cencini, A. Lanotte, S. Musacchio, and F. Toschi, Heavy Particle Concentration in Turbulence at Dissipative and Inertial Scales, *Phys. Rev. Lett.* **98**, 084502 (2007).
- [25] R. Onishi, K. Takahashi, and J. C. Vassilicos, An efficient parallel simulation of interacting inertial particles in homogeneous isotropic turbulence, *J. Comput. Phys.* **242**, 809 (2013).
- [26] G. Boffetta, F. De Lillo, and A. Gamba, Large scale inhomogeneity of inertial particles in turbulent flows, *Phys. Fluids* **16**, L20 (2004).
- [27] H. Yoshimoto and S. Goto, Self-similar clustering of inertial particles in homogeneous turbulence, *J. Fluid Mech.* **577**, 275 (2007).
- [28] R. Monchaux, M. Bourgoïn, and A. Cartellier, Preferential concentration of heavy particles: A Voronoï analysis, *Phys. Fluids* **22**, 103304 (2010).
- [29] E. W. Saw, R. A. Shaw, S. Ayyalasomayajula, P. Y. Chuang, and Á. Gylfason, Inertial Clustering of Particles in High-Reynolds-Number Turbulence, *Phys. Rev. Lett.* **100**, 214501 (2008).
- [30] T. Gotoh and P. K. Yeung, Passive scalar transport in turbulence: A computational perspective, in *Ten Chapters in Turbulence*, edited by P. A. Davidson, Y. Kaneda, and K. R. Sreenivasan (Cambridge University Press, New York, 2013), pp. 87–131.
- [31] T. Ariki, K. Yoshida, K. Matsuda, and K. Yoshimatsu, Scale-similar clustering of heavy particles in the inertial range of turbulence, *Phys. Rev. E* **97**, 033109 (2018).
- [32] S. W. Coleman and J. C. Vassilicos, A unified sweep-stick mechanism to explain particle clustering in two- and three-dimensional homogeneous, isotropic turbulence, *Phys. Fluids* **21**, 113301 (2009).
- [33] S. Goto and J. C. Vassilicos, Self-similar clustering of inertial particles and zero-acceleration points in fully developed two-dimensional turbulence, *Phys. Fluids* **18**, 115103 (2006).
- [34] L. Chen, S. Goto, and J. C. Vassilicos, Turbulent clustering of stagnation points and inertial particles, *J. Fluid Mech.* **553**, 143 (2006).
- [35] S. Goto and J. C. Vassilicos, Sweep-Stick Mechanism of Heavy Particle Clustering in Fluid Turbulence, *Phys. Rev. Lett.* **100**, 054503 (2008).
- [36] A. D. Bragg, P. J. Ireland, and L. R. Collins, Mechanisms for the clustering of inertial particles in the inertial range of isotropic turbulence, *Phys. Rev. E* **92**, 023029 (2015).
- [37] M. Farge and R. Sadourny, Wave-vortex dynamics in rotating shallow water, *J. Fluid Mech.* **206**, 433 (1989).
- [38] M. Farge, Wavelet transforms and their applications to turbulence, *Annu. Rev. Fluid Mech.* **24**, 395 (1992).
- [39] C. Meneveau, Analysis of turbulence in the orthonormal wavelet representation, *J. Fluid Mech.* **232**, 469 (1991).
- [40] M. Farge, K. Schneider, and N. Kevlahan, Non-Gaussianity and coherent vortex simulation for two-dimensional turbulence using an adaptive orthogonal wavelet basis, *Phys. Fluids* **11**, 2187 (1999).
- [41] M. Farge, G. Pellegrino, and K. Schneider, Coherent Vortex Extraction in 3D Turbulent Flows Using Orthogonal Wavelets, *Phys. Rev. Lett.* **87**, 054501 (2001).
- [42] N. Okamoto, K. Yoshimatsu, K. Schneider, M. Farge, and Y. Kaneda, Coherent vortices in high resolution direct numerical simulation of homogeneous isotropic turbulence: A wavelet viewpoint, *Phys. Fluids* **19**, 115109 (2007).
- [43] K. Schneider, M. Farge, and N. Kevlahan, Spatial intermittency in two-dimensional turbulence: A wavelet approach, in *Woods Hole Mathematics, Perspectives in Mathematics and Physics*, edited by N. Tongring and R. C. Penner (World Scientific, Singapore, 2004), Vol. 34, pp. 302–328.

- [44] W. J. Bos, L. Liechtenstein, and K. Schneider, Small-scale intermittency in anisotropic turbulence, *Phys. Rev. E* **76**, 046310 (2007).
- [45] K. Yoshimatsu, N. Okamoto, K. Schneider, Y. Kaneda, and M. Farge, Intermittency and scale-dependent statistics in fully developed turbulence, *Phys. Rev. E* **79**, 026303 (2009).
- [46] M. Farge and K. Schneider, Coherent vortex simulation (CVS), a semi-deterministic turbulence model using wavelets, *Flow, Turbul. Combust.* **66**, 393 (2001).
- [47] K. Schneider, M. Farge, G. Pellegrino, and M. Rogers, Coherent vortex simulation of three-dimensional turbulent mixing layers using orthogonal wavelets, *J. Fluid Mech.* **534**, 39 (2005).
- [48] K. Schneider and O. V. Vasilyev, Wavelet methods in computational fluid dynamics, *Annu. Rev. Fluid Mech.* **42**, 473 (2010).
- [49] J. Urzay, A. Doostmohammadi, and J. M. Yeomans, Multi-scale statistics of turbulence motorized by active matter, *J. Fluid Mech.* **822**, 762 (2017).
- [50] J. Kim, M. Bassenne, C. A. Z. Towery, P. E. Hamlington, A. Y. Poludnenko, and J. Urzay, Spatially localized multi-scale energy transfer in turbulent premixed combustion, *J. Fluid Mech.* **848**, 78 (2018).
- [51] A. Freund and A. Ferrante, Wavelet-spectral analysis of droplet-laden isotropic turbulence, *J. Fluid Mech.* **875**, 914 (2019).
- [52] M. Bassenne, J. Urzay, K. Schneider, and P. Moin, Extraction of coherent clusters and grid adaptation in particle-laden turbulence using wavelet filters, *Phys. Rev. Fluids* **2**, 054301 (2017).
- [53] M. Bassenne, P. Moin, and J. Urzay, Wavelet multiresolution analysis of particle-laden turbulence, *Phys. Rev. Fluids* **3**, 084304 (2018).
- [54] R. Onishi, K. Matsuda, and K. Takahashi, Lagrangian tracking simulation of droplet growth in turbulence—turbulence enhancement of autoconversion rate, *J. Atmos. Sci.* **72**, 2591 (2015).
- [55] Y. Morinishi, T. S. Lund, O. V. Vasilyev, and P. Moin, Fully conservative higher order finite difference schemes for incompressible flow, *J. Comput. Phys.* **143**, 90 (1998).
- [56] C. W. Hirt and J. L. Cook, Calculating three-dimensional flow around structures and over rough terrain, *J. Comput. Phys.* **10**, 324 (1972).
- [57] R. Onishi, Y. Baba, and K. Takahashi, Large-scale forcing with less communication in finite-difference simulations of steady isotropic turbulence, *J. Comput. Phys.* **230**, 4088 (2011).
- [58] R. Nguyen van yen, D. del-Castillo-Negrete, K. Schneider, M. Farge, and G. Chen, Wavelet-based density estimation for noise reduction in plasma simulations using particles, *J. Comput. Phys.* **229**, 2821 (2010).
- [59] I. Daubechies, *Ten Lectures on Wavelets* (Society for Industrial and Applied Mathematics, Philadelphia, 1992).
- [60] S. Mallat, *A Wavelet Tour of Signal Processing. The Sparse Way*, 3rd ed. (Academic Press, Burlington, 2009).
- [61] I. Saito and T. Gotoh, Turbulence and cloud droplets in cumulus clouds, *New J. Phys.* **20**, 023001 (2018).
- [62] V. Dallas and J. C. Vassilicos, Rapid growth of cloud droplets by turbulence, *Phys. Rev. E* **84**, 046315 (2011).
- [63] Y. Sakurai and T. Ishihara, Relationships between small-scale fluid motions and inertial particle clustering in turbulence, *J. Phys. Soc. Jpn.* **87**, 093401 (2018).
- [64] K. Karpińska, J. F. Bodenschatz, S. P. Malinowski, J. L. Nowak, S. Risius, T. Schmeissner, R. A. Shaw, H. Siebert, H. Xi, H. Xu, and E. Bodenschatz, Turbulence-induced cloud voids: Observation and interpretation, *Atmos. Chem. Phys.* **19**, 4991 (2019).
- [65] T. Oujia, K. Matsuda, and K. Schneider, Divergence and convergence of inertial particles in high Reynolds number turbulence, *J. Fluid Mech.* **905**, A14 (2020).
- [66] L. Villafane-Roca, M. Esmaily-Moghadam, A. Banko, and J. K. Eaton, A robust method for quantification of preferential concentration from finite number of particles, Annual Research Briefs 2016 (Center for Turbulence Research, Stanford University, Stanford, 2016), pp. 123–135.